Journal of Catalysis **210,** 97–105 (2002)
doi:10.1006/jcat.2002.3667

In_2O_3/Al_2O_3 Catalysts for NO_x Reduction in Lean Condition

Paul W. Park,*,[1] Christie S. Ragle,* Carrie L. Boyer,* M. Lou Balmer,†,[2]
Mark Engelhard,† and David McCready†

*Caterpillar Inc., Tech Center E/854, P.O. Box 1875, Peoria, Illinois 61656; and †Pacific Northwest National Laboratory, P.O. Box 999, Richland, Washington 99352

Received December 18, 2001; revised April 30, 2002; accepted May 8, 2002

The lean NO_x performance and catalytic properties of In_2O_3/Al_2O_3 catalysts were investigated. High lean NO_x activity was observed when propene was used as a reductant in the presence of 9% O_2 and 7% H_2O at a space velocity of 30,000 h^{-1}. The optimum lean NO_x activity of In_2O_3/Al_2O_3 catalysts was observed at a loading of 2.5 wt% indium on γ-Al_2O_3 which was prepared by a sol–gel technique (230 m^2/g). When propane was used as a reductant, the In_2O_3/Al_2O_3 catalyst did not promote NO_x reduction compared to the alumina substrate. X-ray photoelectron spectroscopy (XPS), X-ray diffraction (XRD), and temperature-programmed reduction (TPR) have been used to characterize a series of In_2O_3/Al_2O_3 catalysts to increase understanding of the surface structure of indium oxide species on the alumina support. The XRD data indicated that crystalline In_2O_3 was present at In_2O_3 loadings >5 wt% and the quantity of the crystalline phase increased as a function of indium loading. XPS results suggested that indium oxide existed as a well-dispersed phase up to 10 wt% indium. The well-dispersed or reducible indium oxide species below 400°C in TPR experiments were assigned as the sites which activate propene to oxygenated hydrocarbons such as acetaldehyde and acrolein. Alumina sites readily utilize the oxygenated hydrocarbons to reduce NO_x. A bifunction mechanism was proposed to explain high NO_x reduction over In_2O_3/Al_2O_3 catalysts.

Key Words: **NO_x; reduction; lean; In_2O_3; Al_2O_3; XPS; XRD; TPR; acrolein; acetaldehyde.**

1. INTRODUCTION

Nitrogen oxides (NO_x) emitted from internal combustion engines are a serious environmental concern. For stationary lean-burn engine applications, NO_x has been effectively controlled by selective catalytic reduction (SCR) with ammonia. However, ammonia SCR technology may not be suitable for mobile applications because it requires a nationwide infrastructure of ammonia or urea supply and needs to address safety issues for handling toxic ammonia. In this respect, a lean NO_x catalyst using onboard fuel to supply hydrocarbon as a reductant has attracted much attention as an alternative technique to conventional NH_3–SCR processes. Cu–ZSM-5 was discovered to be a catalytic material very effective in reducing NO to N_2 (1, 2); however, it has been a great challenge to develop more-effective and -durable catalysts to remove NO_x from diesel or lean-burn gasoline engines.

Zeolite materials show excellent NO_x reduction efficiency especially at high space velocity; however, cation migration and hydrothermal stability limits the application of the materials in practical applications. Noble metal-based catalysts show high NO_x conversion at lower temperatures; however, these catalysts inefficiently utilize reductants and produce N_2O, which is a stable pollutant and a strong greenhouse gas. Base metal oxides supported on alumina catalysts have drawn many researchers' attention because these catalytic materials are highly stable at elevated temperature as well as very selective for NO_x reduction while consuming a minimal amount of reductant.

Indium oxide has shown promise for lean NO_x catalysis. In_2O_3 doped on alumina has been reported to show high-activity NO_x reduction as well as high resistance to water and SO_2 poisoning in lean conditions (3). Kikuchi and co-workers (4–6) introduced indium into various zeolite materials and reported that In/H–ZSM-5 showed higher catalytic activity and selectivity for NO_x reduction than other In-exchanged zeolitic materials when CH_4 was used as a reductant. Hamada and co-workers (7, 8) studied In_2O_3-doped sol–gel alumina catalysts and reported that the catalyst showed better catalytic performance than In- or Cu-exchanged ZSM-5 catalysts. In addition, the indium catalysts showed higher activity for NO reduction over the broad temperature window compared to various metal oxides, such as Sn, Ag, Co, Cu, Fe, and Ni, supported on 30 wt% Ga_2O_3/Al_2O_3 catalysts, especially in the presence of H_2O at low temperature (≤350°C). The authors concluded that the presence of H_2O enhanced the catalytic performance for NO reduction due to suppression of undesirable propene oxidation and to removal of surface carbonaceous materials.

[1] To whom correspondence should be addressed. E-mail: park_paul_w@cat.com.

[2] Current address: Caterpillar Inc., Tech Center E/854, P.O. Box 1875, Peoria, IL 61656.

0021-9517/02 $35.00

Although promising results of indium-based catalysts have been recently reported, the detailed surface structure of indium species on alumina and the role of indium in NO_x reduction have not been investigated. In this paper, we show that an In_2O_3/Al_2O_3 catalyst is one of the most active catalysts for lean NO_x catalysis using a propene reductant in simulated engine exhaust (9% O_2, 7% H_2O, and 30,000 h^{-1} space velocity). XRD (X-ray diffraction), XPS (X-ray photoelectron spectroscopy), and TPR (temperature-programmed reduction) were used to characterize the properties of indium species on alumina. The information derived from the characterization techniques has been correlated with NO_x reduction (NO and NO_2) results using different hydrocarbons (C_3H_6 and C_3H_8). The reaction mechanism and identity of the active sites on these In_2O_3/Al_2O_3 catalysts are proposed.

2. EXPERIMENTAL

2.1. Catalyst Preparation

The alumina support was prepared by a sol–gel method using alumina isopropoxide and 2-methyl-2,4-pentanediol as a complexing agent. The procedure for the alumina preparation was described previously (9). In_2O_3/Al_2O_3 catalysts were prepared using the incipient wetness technique with γ-alumina powder (surface area, 230 m^2/g) and aqueous solutions of indium(III) nitrate pentahydrate (Aldrich, 99.99%). In (2.5 wt%) doped on SiO_2 powder (Aerosil Degussa, 200 m^2/g) was also prepared by an incipient wetness technique to study reaction mechanisms. The impregnated samples were dried in air at 100°C for 24 h and calcined at temperatures up to 600°C (ramp rate, 1.2°C/min) for 5 h under flowing air (5 L/min). The indium content of the In_2O_3/Al_2O_3 series was varied from an In/Al atomic ratio of 0 to 0.128 (0–20 wt% based on In metal). In_2O_3/Al_2O_3 catalysts will be designated "In*y*," where *y* is the In content (weight percent).

2.2. Catalytic Performance Test

The catalytic performance of samples was measured using a quartz microtube reactor system with a feed gas of 0.1% NO_x, 0.1% propene, 9% O_2, and 7% H_2O balanced with He. The total gas flow rate was 200 cc/min, and 0.2 g of catalyst sample was used, unless otherwise noted. The reaction products were measured and identified by GC, GC–MS, or NO_x chemiluminescence analyzer. NO_x conversion was calculated from the amount of N_2 produced. Since no by-product such as N_2O was detected in any of the experiments, the measured N_2 yield corresponded directly to NO_x conversion. The catalyst samples were initially heated to 600°C with 15% O_2/He. When the temperature reached 600°C, H_2O, NO_x, and propene were introduced into the reaction mixture. Activity data was recorded from high temperature to low temperature. To study the roles of In_2O_3 and γ-Al_2O_3, two individual reactors containing each component were installed to a bench system with three-way valves to pass or bypass the reaction mixture so that the products produced over each catalyst bed individually or in series were analyzed.

2.3. BET

Surface area, pore volume, and pore size distribution measurements were performed using a Micromeritics ASAP 2010 system. Catalyst samples were outgassed under vacuum at 450°C overnight prior to taking adsorption measurements. The surface area was determined by multipoint measurements using several relative pressures of N_2 in the range 0.06–0.2 (N_2 surface area, 0.162 nm^2) at 77 K.

2.4. X-Ray Diffraction (XRD)

X-ray powder diffraction patterns were obtained with a Philips PW3040/00 X'Pert MPD system which employed a PW3050/10 vertical theta–theta goniometer and a PW3373 long fine-focus, ceramic X-ray tube with fixed Cu anode. The X-ray source was operated at 2000 W (40 kV, 50 mA). The optical train of the diffractometer consisted of programmable divergence, antiscatter, and receiving slits, a curved graphite monochromator, and a Xe proportional counter detector. The divergence and antiscatter slits were operated in 2-theta compensating mode. Combined with a fixed, 10-mm-wide brass beam mask, the study area on the mounted specimens was limited to 10 mm × 10 mm. The receiving slit was set at 0.2 mm height. The samples were fine-grained, dry powders mounted in 12 mm diameter × 0.5 mm deep cavities cut in off-axis single-crystal quartz plates. The range of diffraction data collection was 10–80° (2-theta), which was scanned at a rate of 0.04°/2 s.

2.5. X-Ray Photoelectron Spectroscopy (XPS)

XPS measurements were made on a Physical Electronics Quantum 2000 Scanning ESCA Microprobe. This system uses a focused monochromatic Al $K\alpha$ X-ray (1486.7 eV) source for excitation and a spherical section analyzer. The X-ray beam used was a 100-W, 100-μm-diameter beam that is rastered over a 1.5 mm by 0.2 mm rectangle on the sample. The X-ray beam is incident normal to the sample and the X-ray detector is at 45° away from normal. The collected data were referenced to an energy scale with binding energies for Cu $2p_{3/2}$ at 932.67 ± 0.05 eV and for Au 4f at 84.0 ± 0.05 eV. Low-energy electrons and argon ions were used for specimen neutralization.

2.6. Temperature-Programmed Reduction (TPR)

Temperature-programmed characterization was performed on an Advanced Scientific Designs Inc. (ASDI) catalyst test stand. Catalyst powder samples (0.1–0.2 g) were placed on a glass frit in a flow-through tube that was

evacuated at 10^{-3} torr. The samples were pretreated to 105°C at 10^{-3} torr for 1 h, then cooled to room temperature under vacuum. For temperature-programmed reduction studies, the sample was exposed to a mixture of 4% H_2 in argon at a flow rate of 10 cc/min. Samples were heat treated at a rate of 10°C/min to 850°C then held at 850°C for 1 h under the flowing H_2/Ar mixture. Hydrogen uptake during heat treatment was measured using a thermal conductivity detector (TCD).

3. RESULTS

3.1. NO_x Reduction over In_2O_3/Al_2O_3 Catalysts

3.1.1. The effect of indium loading on NO_x reduction. In order to determine the optimum loading of indium on the sol–gel alumina support, NO reduction with C_3H_6 was examined over a series of indium-doped alumina catalysts. Figure 1a shows N_2 yields and Fig. 1b integral N_2 production rates as a function of reaction temperature for NO reduction over 1, 2.5, 5, and 10 wt% indium-doped Al_2O_3 catalysts. The NO reduction performance for undoped alumina is also shown in Fig. 1 for comparison. T_{max} (temperature at maximum NO_x conversion) of the alumina for NO reduction was 575°C and the NO conversion at T_{max} was 51%. All of the indium-doped alumina catalysts showed lower T_{max} and exhibited a broader temperature window of operation than those of the undoped alumina. The In2.5 catalyst showed optimum NO reduction performance with the highest N_2 yield (60%). The performance of NO reduction over the In_2O_3/Al_2O_3 catalysts decreased with increasing indium loading, from 2.5 to 10 wt%.

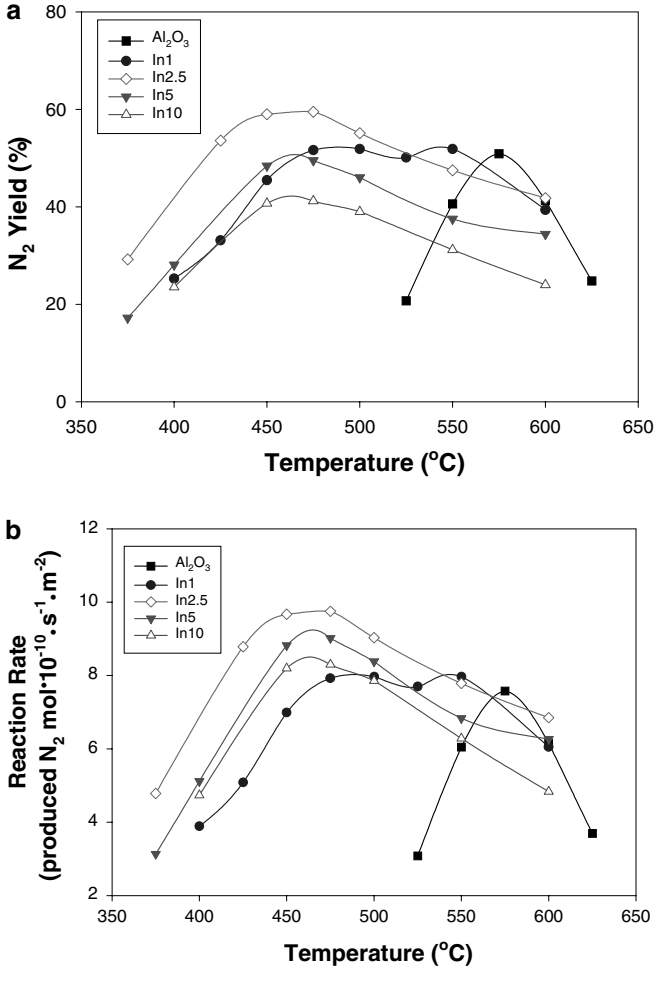

FIG. 1. The effect of indium loading on (a) the N_2 yield and (b) the integral N_2 formation rate normalized by the catalyst surface area for NO reduction over In_2O_3/Al_2O_3 catalysts (0.1% NO, 0.1% C_3H_6, 9% O_2, 7% H_2O, SV = 30,000 h^{-1}).

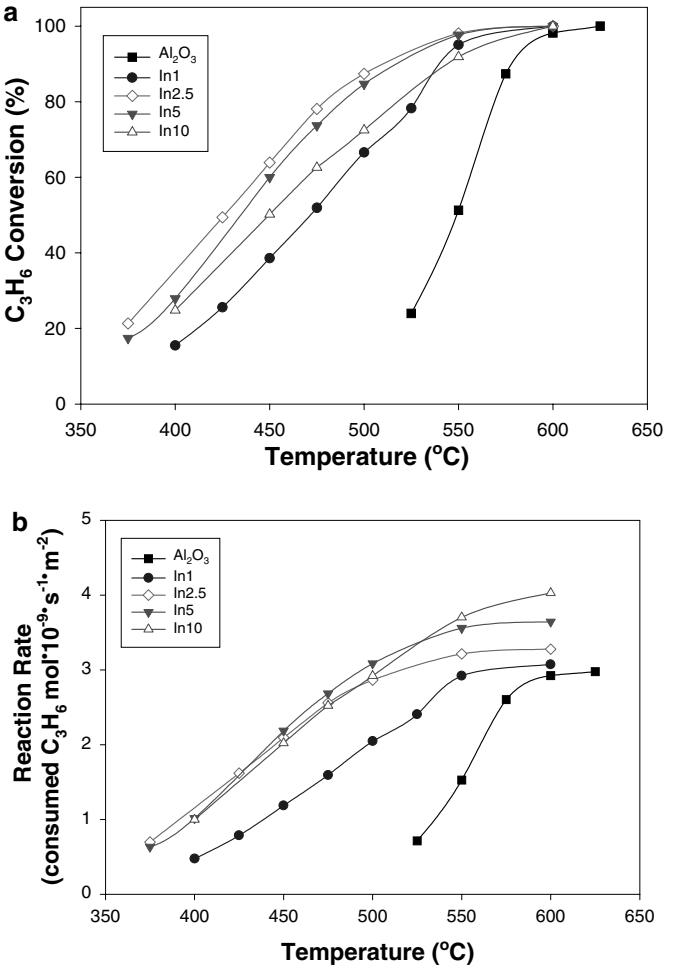

FIG. 2. The effect of indium loading on (a) the C_3H_6 conversion and (b) the integral C_3H_6 consumption rate normalized by the catalyst surface area for NO reduction over In_2O_3/Al_2O_3 catalysts (0.1% NO, 0.1% C_3H_6, 9% O_2, 7% H_2O, SV = 30,000 h^{-1}).

Figure 2a illustrates propene conversions and Fig. 2b integral propene consumption rates as a function of reaction temperature for NO reduction over the catalysts. Undoped alumina, shown on the far right of the graph, converted propene at the rate of 20–100% in the temperature range

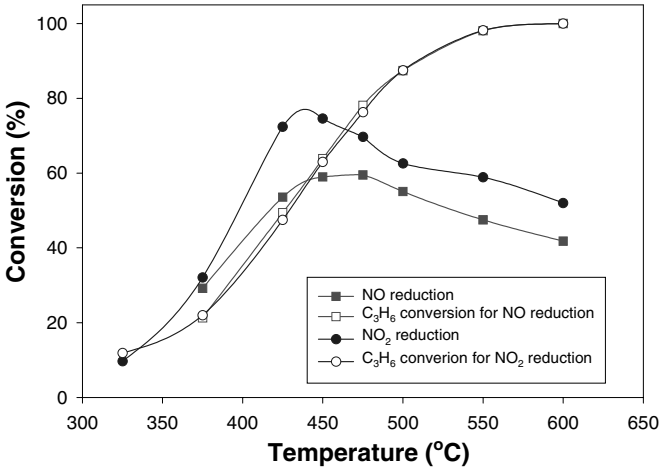

FIG. 3. The effect of NO_x species on NO_x reduction over In2.5 (0.1% NO_x, 0.1% C_3H_6, 9% O_2, 7% H_2O, SV = 30,000 h^{-1}).

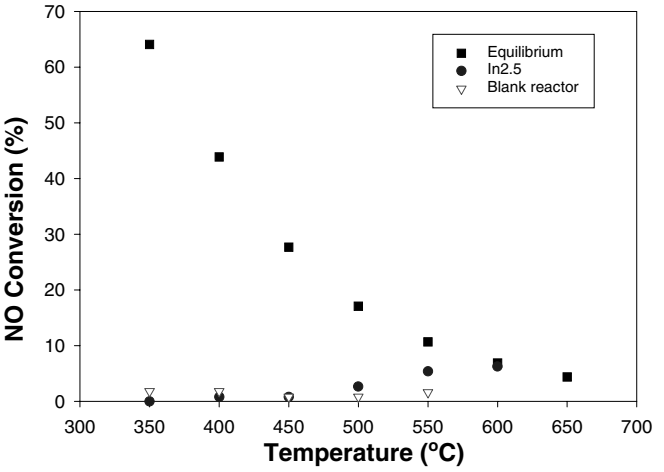

FIG. 4. NO oxidation to NO_2 over In2.5 (0.1% NO, 10% O_2, SV = 25,000 h^{-1}).

525–625°C, respectively. The addition of up to 2.5 wt% indium to the alumina significantly lowered the activation energy for propene conversion, as shown by lower reaction temperatures. Increasing the indium beyond 2.5 to 5 and 10 wt% levels reversed this trend and increased the reaction temperature, thereby increasing the activation energy. However, notice that 100% conversion of propene still occurs at the elevated temperature of 600°C for all catalysts tested.

3.1.2. The effect of NO_x species. Figure 3 compares NO_x reductions and C_3H_6 conversions as a function of temperature over the In2.5 catalyst for NO and NO_2. While the T_{max} and peak shape was similar for NO and NO_2 feeds, the N_2 yield from NO_2 reduction was higher over the entire temperature range. Alternatively, the propene conversion profiles were the same with NO and NO_2 feeds despite the fact that NO_2 is a stronger oxidation agent than NO.

The extent of NO oxidation reaction was measured over the In2.5 catalyst with a feed of 0.1% NO, 10% O_2, and an SV of 25,000 h^{-1} (Fig. 4). The theoretical equilibrium value of NO to NO_2 conversion and the experimentally determined values in an empty reactor under the same reaction conditions are also shown for comparison. The NO oxidation activity over the In2.5 catalyst was negligible and was similar to the blank reactor below 500°C. The NO_2 concentration remained below the equilibrium value even at 550°C.

3.1.3. The effect of hydrocarbon species. Figure 5 compares the NO reduction and hydrocarbon conversions as a function of reaction temperature over the In2.5 catalyst with two hydrocarbon species: C_3H_6 and C_3H_8. Both NO reduction and hydrocarbon conversion were suppressed significantly when C_3H_6 was replaced with C_3H_8. As shown in Fig. 5, the NO reduction peak profile with propane as the reductant was narrower and shifted to higher temperatures by 150°C. In addition, the maximum NO conversion decreased from 60 to 42% when C_3H_6 was replaced with C_3H_8.

Figure 6 illustrates N_2 yield as a function of reaction temperature for NO_x reduction with propane reductant over the indium-doped alumina catalysts. The NO reduction performance for undoped alumina is also shown in Fig. 6 for comparison. In1 and In2.5 catalysts showed NO reduction similar to that of alumina. Increasing the indium to 10 wt% levels decreased NO_x reduction performance to levels even lower than that of alumina. The results of NO_2 reduction with propane (Fig. 6b) over the series of indium-doped aluminas shows that the addition of indium oxide did not promote NO_x reduction and in fact lowered the activity for NO_2 reduction.

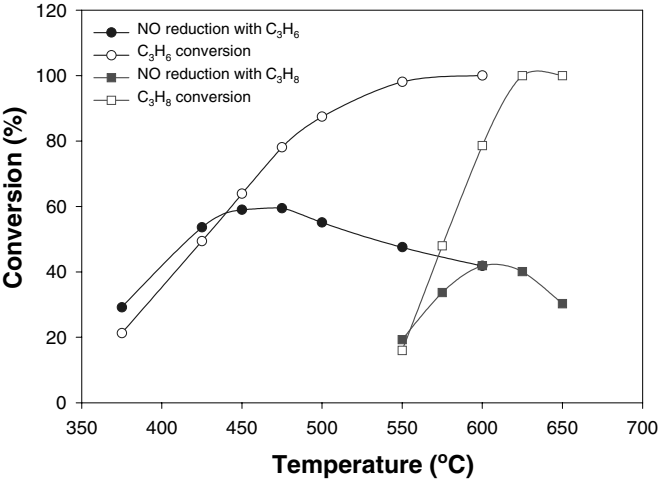

FIG. 5. The effect of hydrocarbon species on NO reduction over In2.5 (0.1% NO, 0.1% C_3H_x, 9% O_2, 7% H_2O, SV = 30,000 h^{-1}).

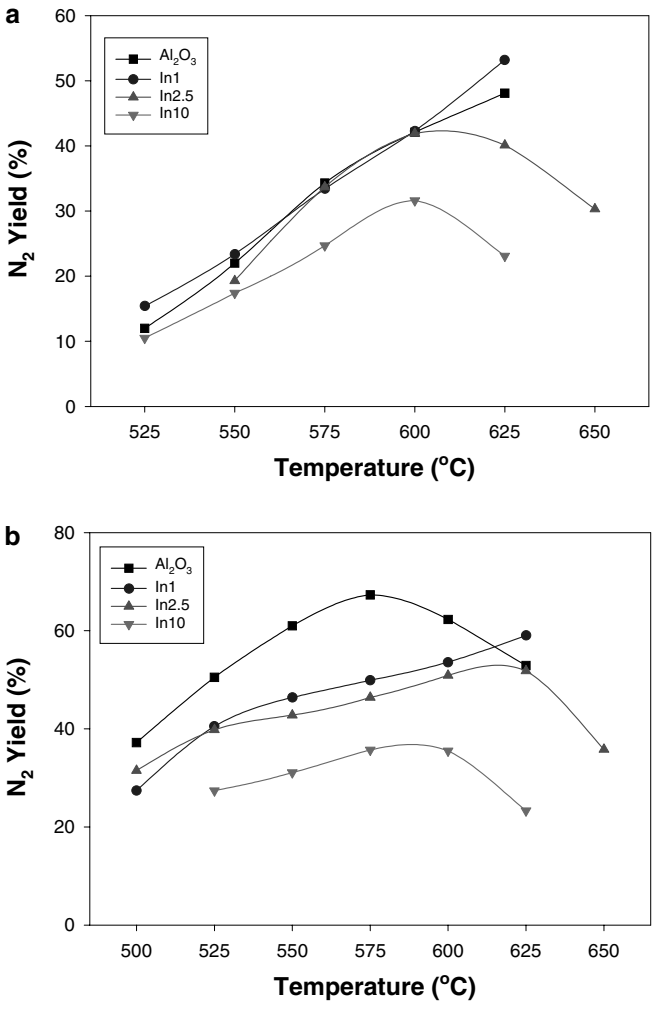

FIG. 6. The effect of indium loading on N_2 yield for (a) NO reduction and (b) NO_2 reduction with C_3H_8 over In_2O_3/Al_2O_3 catalysts (0.1% NO, 0.1% C_3H_8, 9% O_2, 7% H_2O, SV = 30,000 h^{-1}).

3.1.4. The role of indium oxide. In order to elucidate the individual roles of In_2O_3 and of Al_2O_3, an experiment was performed using a dual-bed reactor system in which the components were separately loaded in two catalyst beds arranged in series and the products over each catalyst bed were analyzed. SiO_2 was used to support the In_2O_3 because it is expected to be inert for hydrocarbon oxidation and NO_x reduction.

Table 1 shows reaction products over a single-bed catalyst of 0.1 g In2.5/Al_2O_3, 0.3 g In2.5/SiO_2, and 0.1 g Al_2O_3, as well as over dual-bed catalysts, which the reaction mixture passed through 0.3 g In2.5/SiO_2 catalyst and then through 0.1 g Al_2O_3. The 0.1-g In2.5/Al_2O_3 catalyst demonstrated excellent NO reduction (54%) and hydrocarbon conversion (67%) in the presence of 9% O_2 and 7% H_2O at a high space velocity of 60,000 h^{-1}.

However, when the same loading of indium (2.5 wt%) was introduced on SiO_2 support, no N_2 formation was detected despite 23% propene conversion. Instead, 16 ppm acrolein (C_3H_4O) and 22 ppm acetaldehyde (CH_3CHO) were observed over the In2.5/SiO_2 catalyst.

Alumina was tested at higher temperatures (500°C) than were In2.5/Al_2O_3 or In2.5/SiO_2 catalysts; however, the alumina converted only 4% NO to N_2 and 3% propene to CO and CO_2. No acrolein or acetaldehyde was observed. This indicates that alumina alone did not contribute significantly to NO and propene conversions at the reaction temperature.

When the alumina was placed downstream of the In2.5/SiO_2 catalyst, NO reduction to N_2 (59 ppm) increased by a factor of 3 compared to that with alumina alone. Acrolein and acetaldehyde produced over the In2.5/SiO_2 catalyst was not observed after the alumina. The overall propene conversion over a dual-bed catalyst was similar to In2.5/SiO_2; therefore, most of hydrocarbon was activated over indium species.

Table 2 shows major reaction products over the In2.5/SiO_2 catalyst when each oxidant (O_2, NO, or NO_2) was introduced individually in the gas stream in order to identify the origin of oxygen in the produced acetaldehyde and acrolein. Substantial propene conversions (>16%) and production of acetaldehyde, acrolein, CO, and CO_2 were observed when O_2 or NO_2 was used as oxidation agents. However, no oxygenated hydrocarbon was observed with a minimum propene conversion when NO was used. The results indicate that the oxygen atoms in the oxygenated hydrocarbons are originally from O_2.

TABLE 1

The Results of GC/MS Analysis for NO Reduction over In Catalysts and γ-Al_2O_3

	Product concentration (ppm)						Conversion (%)		
Catalyst	N_2	CO	CO_2	C_3H_6	CH_3CHO	CH_2=CHCHO	C_3H_6	NO	Temperature (°C)
In2.5/Al_2O_3	272	469	1314	300	0	0	67	54	475
In2.5/SiO_2	0	96	432	824	22	16	23	0	475
Al_2O_3	21	75	19	1040	0	0	3	4	500
In2.5/SiO_2 + Al_2O_3	59	332	444	811	0	0	24	12	475
									500

Note. Reaction condition: 1000 ppm NO, 1060 ppm C_3H_6, 9% O_2, 7% H_2O, balanced with He; total flow, 200 cc/min.

TABLE 2

The Results of GC/MS Analysis over an In2.5/SiO_2 Catalyst

Gas mixture	Product concentration (ppm)					Conversion (%)
	CO	CO_2	C_3H_6	CH_3CHO	CH_2=CHCHO	
$O_2 + C_3H_6 + He$	246	286	854	9.7	12.7	17.6
$NO + C_3H_6 + He$	0	6	1019	0	0	1.6
$NO_2 + C_3H_6 + He$	115	265	865	2.8	21.2	16.5

Note. Reaction condition: 940 ppm NO, 970 ppm NO_2 or 9.3% O_2 in the presence of 1040 ppm C_3H_6, balanced with He; total flow, 200 cc/min; reaction temperature, 475°C.

3.2. Catalyst Characterization

Table 3 shows BET results of the In_2O_3/Al_2O_3 catalysts. The surface area, pore volume, and pore diameter of the catalysts significantly decreased as a function of indium content. The decrease in surface area, pore volume, and pore diameter was not proportional to the increase in indium content on the alumina support. For example, for the In15 catalyst, the percentage loss of surface area (37%), pore volume (69%), and pore diameter (52%) based on the alumina was more than the percentage increase in indium loading (15%).

Figure 7 shows powder XRD patterns of the In_2O_3/Al_2O_3 catalysts. The diffraction patterns for samples containing up to In2.5 are characteristic of the alumina support. However, XRD patterns obtained for samples with indium loadings higher than 5 wt% contained peaks characteristic of In_2O_3 in addition to alumina peaks. The intensities of the In_2O_3 XRD peaks increased with increasing indium content. XRD patterns that were measured after the same catalysts were used for lean NO_x reactions showed no difference between fresh and used catalysts (not shown). Therefore, exposure to reaction conditions did not affect the In_2O_3 crystalline phase or the alumina support.

Figure 8 shows the variation of the XPS $In3d_{5/2}$/Al2p intensity ratio measured for the In_2O_3/Al_2O_3 catalysts as a function of In/Al atomic ratio. The intensity ratio of $In3d_{5/2}$/Al2p calculated for theoretical atomic dispersion is also shown for comparison. The theoretical value was cal-

TABLE 3

Surface Area, Pore Volume, and Pore Diameter of In-Doped Alumina Catalysts

Catalysts	Surface area (m^2/g)	Pore volume (cc/g)	Pore diameter (nm)
Al_2O_3	230	1.1	14
In1	223	0.75	10
In2.5	209	0.79	11.3
In5	188	0.58	9.2
In10	170	0.46	7.9
In15	146	0.34	6.7

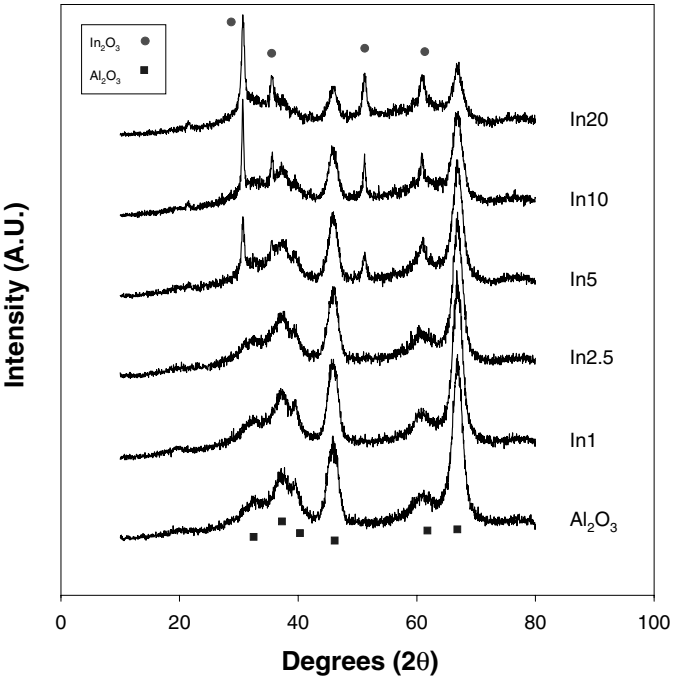

FIG. 7. XRD patterns of In_2O_3/Al_2O_3 catalysts.

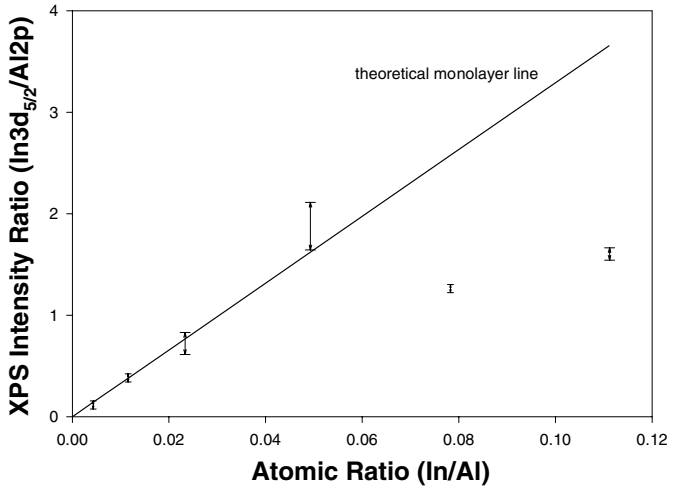

FIG. 8. XPS $In3d_{5/2}$/Al2p intensity ratios measured for In_2O_3/Al_2O_3 catalysts. The theoretical monolayer line is included for comparison.

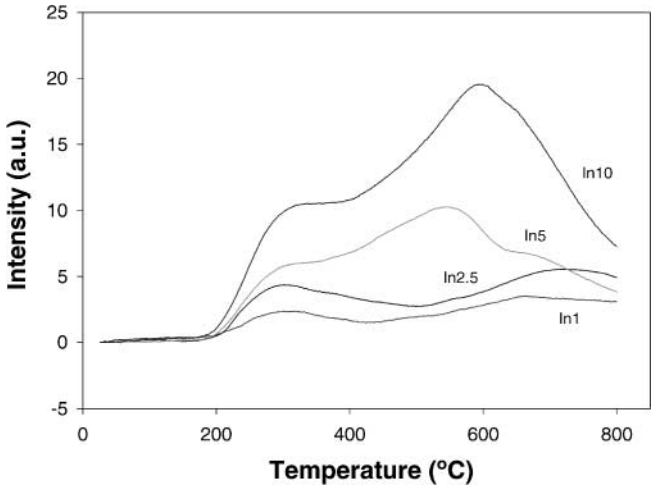

FIG. 9. TPR spectra of In_2O_3/Al_2O_3 catalysts.

culated using the model proposed by Kerkhof and Moulijn (10). The photoelectron cross sections and the mean escape depth of the photoelectrons used in these calculations were taken from Scofield (11) and Penn (12), respectively.

The In/Al intensity ratio increased linearly with increasing In/Al atomic ratio up to 0.049 (In10), consistent with a theoretical monolayer. For higher-indium-loading catalysts (In15 and In20), the In/Al intensity ratios deviated from the linear trend. The In/Al intensity ratios of the catalysts which were tested for the lean NO_x reaction showed similar values and a similar trend within the range of error. Therefore, exposure to reaction conditions did not affect the indium dispersion over the alumina support. The dispersions of indium species were determined by comparing the XPS intensity ratios obtained from the experiments with the values calculated from the theoretical monolayer line. The XPS results indicated that the dispersion of indium species was 100% for In10. However, the dispersion decreased at higher-indium-loading catalysts: 48 and 42% dispersion for In15 and In20, respectively.

Figure 9 shows temperature-programmed reduction spectra for the In_2O_3/Al_2O_3 catalysts. Detectable H_2 uptake was observed at 300 and 675–700°C for In1 and In2.5 catalysts. For the higher-indium-loading catalysts (In5 and In10), an additional H_2 uptake peak was observed in the temperature range of 550–600°C. The H_2 consumption increased as a function of indium loading. From the comparison with the TPR spectra of standard mixtures of In_2O_3 and alumina, the H_2 uptake peaks around 550–600°C can be assigned to the reduction of the large-grained In_2O_3 crystalline phase. The H_2 uptake peak at 300°C was assigned to the reduction of the highly dispersed indium oxide species. The calculation of the amount of H_2 update for each catalyst indicated that 100% of the indium oxide species was reduced to indium metal up to In5. In10 showed 83% of indium oxide to be reduced to the metal during TPR measurements.

Figure 10 shows SEM backscattered images of the In_2O_3/Al_2O_3 catalysts. At indium loadings of less than 2.5 wt%, only the alumina was imaged with the SEM. However, EDS quantitative analysis verified that the concentration of indium was consistent with as-prepared values. At 5 wt% indium loading, well-dispersed particles of indium smaller than 20 nm in diameter (lighter phase) were

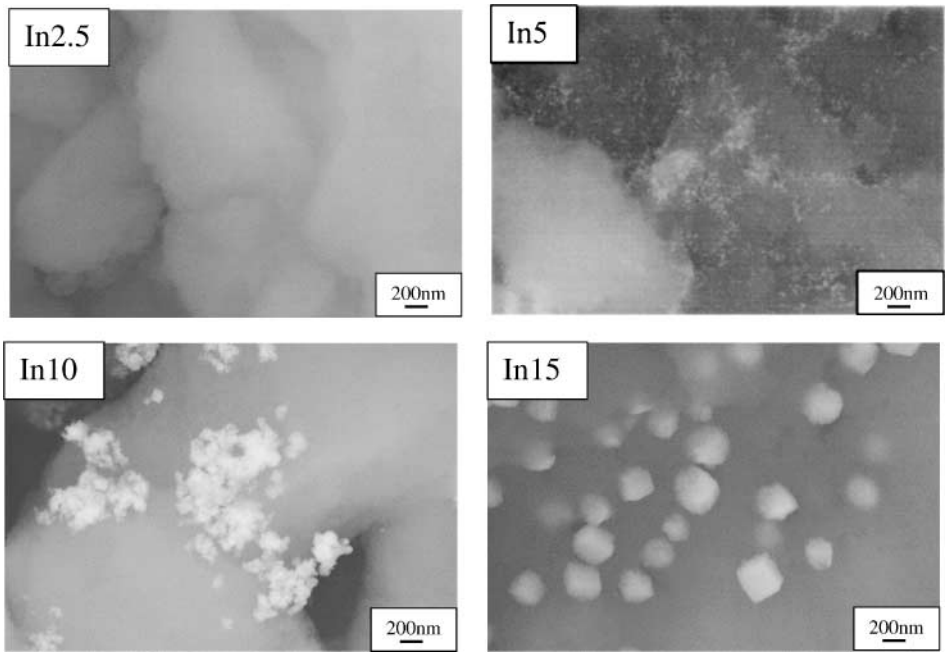

FIG. 10. SEM backscattered images of In_2O_3/Al_2O_3 catalysts.

imaged on the surface of the alumina. The size of the indium species increased with increasing indium content in the sample. At 15 wt% indium loading, large (200 nm)-faceted cubic indium oxide crystallites were observed on the surface.

4. DISCUSSION

The NO_x reduction activity of the most active composition identified in this study, $In2.5/Al_2O_3$, is among the highest reported for the relatively aggressive reaction conditions used in this study (7% H_2O, 9% O_2, and space velocity of 30,000 h^{-1}). The lean NO_x performance of the catalysts was strongly dependent on indium loading similar to other lean NO_x catalysts reported in the literature (Fig. 1). For example, NO conversions over CoO_x/Al_2O_3 and AgO/Al_2O_3 catalysts decrease with increasing metal loading (13, 14). Typically, high metal or metal oxide loading accelerates hydrocarbon oxidation and depletes the reductant, which in turn decreases the catalytic NO_x reduction performance. However, In_2O_3/Al_2O_3 catalysts examined in this study show both a decrease in propene oxidation and a NO reduction at higher indium loadings (Fig. 2). The catalytic performance and characterization results suggest that small, amorphous indium oxide clusters which are present at lower loadings promote NO_x reduction and hydrocarbon oxidation, while larger, crystalline In_2O_3 observed above loadings of 5 wt% (Fig. 7) are less effective for these reactions. As shown in Table 3, alumina parameters such as surface area, pore volume, and average pore diameter decrease significantly with increasing indium loading. While the surface area of the metal oxide is expected to be very small compared to that of the alumina substrate, the observed decrease in the physical properties is larger than predicted by a simple rule of mixtures. This indicates that much of the previously accessible alumina surface area and porosity is blocked by the indium oxide. Therefore, the decrease in catalytic NO_x reduction performance at high indium oxide loadings can be attributed to the reduction in active alumina sites rather than to the acceleration of hydrocarbon oxidation.

In contrast to the findings in this study, Hamada and co-workers found relatively little effect of indium loading on NO reduction with C_3H_6 (7, 8). They observed no significant change in the maximum NO conversion for a range of indium loadings on alumina. However, as shown in Fig. 1, in our study an optimum indium loading (2.5 wt% indium on alumina) was clearly observed for both NO reduction and C_3H_6 conversion. The discrepancy between the two studies can be explained by the difference in reaction conditions. In Hamada's experiments, the contact time was $0.18\ g \cdot s^{-1} \cdot cm^{-3}$, which is three times longer than that used in our work ($0.06\ g \cdot s^{-1} \cdot cm^{-3}$). Due to the relatively mild reaction conditions used in Hamada's study, a significant change in catalytic performance for different indium loadings due to the reduction of alumina sites would be difficult to observe.

The formation of NO_2 and its subsequent reaction with hydrocarbons has been demonstrated to be a key reaction mechanism in lean NO_x catalysis (15–17). It is expected that NO_2 should enhance hydrocarbon conversion compared to NO because NO_2 is a stronger oxidizer. However, C_3H_6 conversion over In2.5 is unchanged when NO is replaced with NO_2 in the gas stream (Fig. 3). This observation suggests that NO_2 does not play a critical role in hydrocarbon activation over this catalyst. Indeed, there is enhancement of NO_x reduction over the entire temperature range when NO is replaced with NO_2. However, this enhancement can be attributed to activity on the Al_2O_3 sites because pure Al_2O_3 is known to be active in promoting the reduction of NO_2 to N_2 by C_3H_6 (9). Al_2O_3 sites should be readily available in the In2.5 catalyst due to the low metal loading. Poor NO oxidation to NO_2 over the In2.5 catalyst (Fig. 4) also suggests that NO_2 plays a minimum role in enhancing catalytic NO_x reduction over the In2.5 composition compared to undoped alumina.

Indium-doped alumina catalysts were further examined with propane in order to understand an essential step in the lean NO_x process (Figs. 5 and 6). The NO_x reduction and hydrocarbon oxidation activity of the In2.5 catalyst was compared using propane and propene as reductants (Fig. 5). The lower lean NO_x activity for propane over the In2.5 catalyst indicates that the catalyst does not promote NO reduction with C_3H_8. With increasing indium loading, the NO reduction performance with C_3H_8 decreased to values even lower than those observed for the alumina support (Fig. 6a). This result indicates that the indium oxide does not utilize propane for NO_x reduction and that it only blocks active sites on the alumina. When NO is replaced with NO_2 with a propane reductant, the catalytic performance did not improve (Fig. 6b). It has been reported that the NO_x reduction over In/H-ZSM-5 catalyst with methane was affected by the species of NO_x and NO_2 was involved in the important reaction mechanism (5). The results obtained in this study indicate that type of hydrocarbon reductant is more critical than NO_x species to achieve high catalytic performance for NO_x reduction over the In_2O_3/Al_2O_3 catalysts.

The role of In_2O_3 in hydrocarbon activation was further proved by quantitative analysis using GC mass spectroscopy over In_2O_3 on an inert substrate (SiO_2). In these experiments, acrolein and acetaldehyde were detected in the exhaust stream after the $In2.5/SiO_2$ catalyst. An alumina catalyst downstream then converted these oxygenated hydrocarbons in a reaction with NO to make N_2 and CO (Table 1). The oxygenated hydrocarbons have also been reported as key intermediates in the selective reduction of NO_x over SnO_2/Al_2O_3 catalysts (18). The authors proposed a bifunction mechanism in which SnO_2 converted propene

to the oxygenated intermediates and Al_2O_3 reduced NO_x to N_2 utilizing these intermediates as reductants. In this study, the same bifunction mechanism is operative over In_2O_3/Al_2O_3 catalysts. Observation of the formation of acrolein and acetaldehyde from hydrocarbon reductants verifies that partial oxidation of the hydrocarbon is more essential for the promotion of NO_x reduction over indium-doped alumina catalysts than is the oxidation of NO to NO_2.

XRD, XPS, and TPR results showed that the dispersion as well as the phase of indium oxide changed as a function of indium loading. The XPS peak intensity ratio of $In3d_{5/2}$/Al2p suggested the indium oxide species were atomically dispersed up to concentrations as high as 10 wt%. However, crystalline In_2O_3 was observed in compositions containing more than 5 wt% indium, indicating that the dispersion was compromised. This can be explained by considering the nature of indium oxide species that can contribute to both XPS and XRD intensities. SEM backscattered images of the catalysts (Fig. 10) showed that dispersed indium clusters and large crystalline indium species were present together on the In5 and In10 catalysts. TPR results confirmed the presence of two different indium oxide species on the alumina support for compositions containing greater than 2.5 wt% indium. For the In5 and In10 catalysts, the presence of the large high-temperature H_2 uptake (550°C) is consistent with XRD data showing that large crystalline In_2O_3 is present in these samples. The low-temperature H_2 uptake (300°C) was assigned to the well-dispersed indium oxide species. The well-dispersed phase increased with increasing indium loading. This finding was consistent with the XPS intensity ratio that increased as a function of indium loading up to the In10 catalyst. XPS and TPR results concluded that the atomically dispersed indium oxide species increased with indium loading up to the In10 catalyst; however, crystallites of In_2O_3 are also present in the catalysts containing higher than 5 wt% indium.

The correlating NO_x performance results and characterization data indicate that the well-dispersed indium oxide species promotes the lean NO_x reaction via partial oxidation of hydrocarbons. However, high concentrations of the well-dispersed indium species on the surface decrease the NO_x reduction activity by blocking active alumina sites. Therefore, it is important to optimize the indium and alumina sites to achieve the best catalytic performance over this class of catalysts.

5. CONCLUSION

Indium (1–10 wt% In) supported sol–gel alumina catalysts converted as much as 60% NO and 70% NO_2 to N_2 in lean exhaust conditions (1000 ppm NO_x, 9% O_2, 7% H_2O, and 30,000 h^{-1} space velocity) with 1000 ppm propene as a reductant. However, with propane as the reductant the activity was diminished to 42% NO conversion. Optimum NO_x reduction activity was achieved with 2.5 wt% indium loadings on alumina (230 m^2/g) prepared by a sol–gel method. This study showed that it is necessary to balance the well-dispersed indium species and alumina active sites in order to achieve the optimum catalytic performance. A bifunction mechanism where the indium oxide species partially oxidizes propene to acrolein and acetaldehyde and the alumina utilizes the oxygenated hydrocarbons to reduce NO_x to N_2 was identified. Characterization results indicated that well-dispersed and readily reducible indium oxide clusters are the active sites for converting propene to the oxygenated hydrocarbons. However, the lean NO_x performance decreases at high indium loadings (>5 wt%) where active alumina sites responsible for NO_x reduction are blocked by well-dispersed indium oxide species.

ACKNOWLEDGMENTS

The research described in this paper was performed in part at the W. R. Wiley Environmental Molecular Sciences Laboratory, a national scientific user facility sponsored by the U.S. Department of Energy's Office of Biological and Environmental Research, located at the Pacific Northwest National Laboratory in Richland, WA. A part of the study was financially supported by the Office of Heavy Vehicle Technologies in the U.S. Department of Energy. The authors also acknowledge Prof. Harold Kung and Prof. Mayfair Kung at Northwestern University for their comments as well as technical support.

REFERENCES

1. Held, W., Konig, A., Richter, T., and Puppe, L., *SAE Paper* 900496 (1990).
2. Iwamoto, M., Yahiro, H., Yuu, Y., Shundo, S., and Mizuno, N., *Shokubai (Catalyst)* **32**, 430 (1990).
3. Miyadera, T., and Yoshida, K., *Chem. Lett.* 1483 (1993).
4. Ogura, M., and Kikuchi, E., *Chem. Lett.* 1017 (1996).
5. Kikuchi, E., Ogura, M., Aratani, N., Sugiura, Y., Hiromoto, S., and Yogo, K., *Catal. Today* **27**, 35 (1996).
6. Ogura, M., Hayashi, M., and Kikuchi, E., *Catal. Today* **45**, 139 (1998).
7. Haneda, M., Kintaichi, Y., and Hamada, H., *Catal. Lett.* **55**, 47 (1998).
8. Maunula, T., Kintaichi, Y., Inaba, M., Haneda, M., Sato, K., and Hamada, H., *Appl. Catal. B* **15**, 291 (1998).
9. Park, P. W., Kung, H. H., Kim, D.-W., and Kung, M. C., *J. Catal.* **184**, 440 (1999).
10. Kerkhof, F. P. J. M., and Moulijn, J. A., *J. Phys. Chem.* **83**, 1612 (1979).
11. Scofield, J. H., *J. Electron. Spectrosc. Relat. Phenom.* **8**, 129 (1976).
12. Penn, D. R., *J. Electron Spectrosc. Relat. Phenom.* **9**, 29 (1976).
13. Yang, J., Kung, M. C., Sachtler, W. M. H., and Kung, H. H., *J. Catal.* **172**, 178 (1997).
14. Bethke, K. A., and Kung, H. H., *J. Catal.* **172**, 93 (1997).
15. Sasaki, M., Hamada, H., Kintaichi, Y., and Takehiko, I., *Catal. Lett.* **15**, 297 (1992).
16. Bethke, K. A., Li, C., Kung, M. C., Yang, B., and Kung, H. H., *Catal. Lett.* **31**, 287 (1995).
17. Lukyanov, D. B., Sill, G., d'Itri, J. L., and Hall, W. K., *J. Catal.* **153**, 265 (1995).
18. Yezerets, A., Zheng, Y., Park, P. W., Kung, M. C., and Kung, H. H., *Stud. Surf. Sci. Catal.* **130**, 629 (2000).